Chapter 1

Nanostructured Thermoelectric Chalcogenides

Javier Gainza, Federico Serrano-Sánchez,
Mouna Gharsallah, Manuel Funes, Félix Carrascoso,
Norbert M. Nemes, Oscar J. Dura,
José L. Martínez and José A. Alonso

Additional information is available at the end of the chapter

http://dx.doi.org/10.5772/intechopen.75442

Abstract

Thermoelectric materials are outstanding to transform temperature differences directly and reversibly into electrical voltage. Exploiting waste heat recovery as a source of power generation could help towards energy sustainability. Recently, the SnSe semiconductor was identified, in single-crystal form, as a mid-temperature thermoelectric material with record high figure of merit, high power factor and surprisingly low thermal conductivity. We describe the preparation of polycrystals of alloys of SnSe obtained by arc-melting; a rapid synthesis that results in strongly nanostructured samples with low thermal conductivity, advantageous for thermoelectricity, approaching the amorphous limit, around 0.3–0.5 W/mK. An initial screening of novel samples $Sn_{1-x}M_xSe$, by alloying with 3d and 4d transition metals such as M = Mn, Y, Ag, Mo, Cd or Au, provides for a means to optimize the power factor. M=Mo, Ag, with excellent values, are described in detail with characterization by x-ray powder diffraction (XRD), scanning electron microscopy (SEM), and electronic and thermal transport measurements. Rietveld analysis of XRD data demonstrates near-perfect stoichiometries of the above-mentioned alloys. SEM analysis shows stacking of nanosized sheets, with large surfaces parallel to layered slabs. An apparatus was developed for the simultaneous measurement of the Seebeck coefficient and electric conductivity at elevated temperatures.

Keywords: thermoelectrics, nanostructuration, lattice thermal conductivity, thermopower, SnSe alloying

1. Introduction

Thermoelectric materials hold a tantalizing promise of greater energy efficiency by providing a robust and clean option for waste heat recovery and conversion to useful electrical energy through the Seebeck effect [1–5]. However, existing materials have poor thermoelectric efficiency. This is related to the inherent difficulty to obtain, at the same time, a high electrical conductivity, a low thermal one, and a very high Seebeck voltage. Thermoelectric materials are characterized, for research purposes, by the thermoelectric figure of merit, $zT = \frac{\sigma S^2}{\kappa} T$, combining into a dimensionless number the Seebeck coefficient, S (the larger, the better), the electrical conductivity, σ (the larger, the better, to minimize waste through Joule-heating), the thermal conductivity, κ (the smaller, the better, to minimize thermally shorting the temperature gradient giving the Seebeck voltage), and the absolute temperature, T. Unfortunately, the character of these properties pulls against the optimization of the figure of merit. While σ is directly proportional to the carrier concentration n, the Seebeck coefficient is inversely proportional to it ($n^{-2/3}$), a common rule for doped semiconductors known since the 1950s as the Pisarenko relation, after Mr. N. L. Pisarenko [6]. Moreover, the Wiedemann-Franz law establishes a direct relationship between σ and the electronic contribution to the thermal conductivity (κ_{ele}) [7, 8]. Usually, the thermoelectric properties are described as:

$$S = \frac{8\pi^2 k_B^2 m^* T}{3e h^2} \left(\frac{\pi}{3n}\right)^{\frac{2}{3}} \tag{1}$$

$$\sigma = \mu e n \tag{2}$$

$$\kappa_{tot} = \kappa_{latt} + \kappa_{ele} = L\sigma T = L\mu e n T \tag{3}$$

A zT above 4 would be desirable for economically viable thermoelectric modules for waste heat recovery, for example, in automotive applications. Yet, current state-of-the-art materials have zT limited to around 2, with commercial materials limited to 1. Furthermore, p- and n-type thermoelectric materials with similar figure of merit, and electrical, thermal, and mechanical characteristics, in the same temperature range are necessary for their implementation. Nonetheless, much effort has gone into developing cost-effective devices for different applications [9–12]. For instance, as potential candidates for gas heat recovery, automobile exhaust thermoelectric generators (AETEG) were first studied in 1963, and they have been thoroughly investigated since then reaching 400 W and 5% efficiency in current Bi_2Te_3-based modules [12–14]. A recent report on AETEG for military SUV applications shows an output power up to 646 W and 1.03% efficiency, which meets the electrical requirements for automotive applications [13]. Another applicability of thermoelectric modules is found as Solar-Heat-Pipe-Thermoelectric-Generator hybrid systems for combined power generation and hot water production in the high-temperature range [11].

Thermoelectric materials are typically degenerately doped semiconductors, often of heavy p-block elements, such as SiGe, Bi_2Te_3, PbTe, and $CoSb_3$ [15–17]. However, recently, a zT as

large as 2.6 was reported above 900 K in an overlooked semiconductor, SnSe [18]. This value was found in a single crystal of SnSe along one crystallographic direction, above a structural phase transition, just below the melting point. Later reports in single crystals found smaller values, and in polycrystalline samples only zT = 1.0 [19–21]. Nevertheless, SnSe is a very promising thermoelectric. As a semiconductor, SnSe was disregarded due to its complicated orthorhombic structure. It consists of puckered layers, quite analogous to black phosphorus, and it has a small bandgap of 0.61 eV, quite sought after among optoelectronic 2D materials [22].

One reason for the high zT of SnSe has to do with its low thermal conductivity. Nevertheless, a further reduction by nanostructuring is highly desirable. According to the Wiedemann-Franz law [7], the thermal conductivity of SnSe is overwhelmingly determined by the lattice thermal conductivity because of its inherently low electrical conductivity. Thus, doping can be used to increase σ through the charge density, and in turn zT. However, following the Pisarenko relation [23], the Seebeck coefficient will decrease with increasing charge concentration. Thus, an optimum must be found of the power-factor, σS^2. Furthermore, an intense controversy arose about the actual thermal conductivity of the material, with values reported anywhere between 0.2 and 1.0 W m^{-1} K^{-1} [18, 19, 21, 24–31]. Numerous different explanations have been proposed for such values, as surface oxidation, exact stoichiometry, porosity, morphology, and crystal defects of the samples. Thermoelectric devices made of this material have not been described yet despite the fact that SnSe presents one of the highest figures of merit, and only a few attempts proving the interface bonding properties for high-temperature modules have been reported [32, 33].

There have been several reports on doped SnSe, with silver, iodine, bismuth, or sodium [19–21, 24, 34, 35]. These can be used to select the type of carriers, since a useful thermoelectric device must contain both p- and n-type thermo-elements. What is common in these studies is that the dopant concentration reaches no more than a few percent. Our group has reported on alloying SnSe with p-block elements, such as Ge, In, and Pb, using arc-melting [36–39]. The arc-melting technique has several advantages for SnSe, and some drawbacks. It is a very fast, one-step synthesis method that avoids the costly and time-consuming steps of spark plasma sintering (SPS), yet produces dense pellets [40]. Crucially, it yields highly nanostructured materials because of the rapid melting and quenching. It also allows for alloying at much higher concentrations. As a drawback, we find our polycrystalline samples to have notoriously low electrical conductivity at room temperature, and also much lower charge carrier density than would be expected from the huge amount of dopants. These are likely related to surface oxidation of the grain boundaries and to charge-trapping at defects.

Here we report on a general survey of alloying SnSe with *d*-block elements. As a quick screening tool, we employed the room temperature Seebeck coefficient and electrical conductivity. As a rule of thumb, we looked for indications of the Pisarenko relation at work: dopants that, at some concentration, can yield highly conducting samples, usually with almost zero Seebeck coefficient, whereas the pure or lightly doped SnSe is a bad conductor with large Seebeck effect. We characterized every composition by laboratory x-ray diffraction to check for phase purity and changes in the lattice constant, a good indication that some of the dopants indeed entered the crystal structure. For some samples, we also measured the Seebeck coefficient and

electrical conductivity at high temperatures (a much more laborious task), where SnSe would perform as a thermoelectric. In particular, we looked for n-type alloys with negative Seebeck coefficient. We also characterized the thermal conductivity of a few selected samples.

2. Experimental section

2.1. Preparation by arc-melting

Tin selenide alloys with various dopings were prepared in an Edmund Buhler mini-arc MAM-1 furnace (**Figure 1a**). Stoichiometric amounts of ground mixture of reacting elements were pelletized in a glove box. Pellets were molten under Ar atmosphere in a water-cooled Cu crucible (**Figure 1b**), leading to ingots of intermetallic characteristics (**Figure 1c**), which were partially ground to powder for structural characterization. The Seebeck coefficient and electrical and thermal conductivities were measured in disk-shaped specimens obtained by pressing the arc-molten ingots under 200 MPa at ambient temperature in a cylindrical die.

2.2. Structural characterization

Laboratory x-ray diffraction (XRD) was used to characterize the as grown samples (in powder form), for phase identification and for assessment of the phase purity, using a Brucker D8 diffractometer (40 kV, 30 mA), controlled by a DIFFRACTPLUS software, in Bragg-Brentano reflection geometry with CuKα radiation (λ = 1.5418 Å), between 10 and 64° in 2θ°. The resulting diffractograms were evaluated by Rietveld method with the FULLPROF program [41]. A pseudo-Voigt profile function was used for the line shape of the diffraction peaks. The following parameters were refined: half-width, pseudo-Voigt, zero shift, background points, and scale factor. Crucially, unit-cell parameters and positional and overall thermal displacement parameters were also refined for XRD data. A preferred orientation correction was applied, considering platelets perpendicular to [100] direction for SnSe-related alloys.

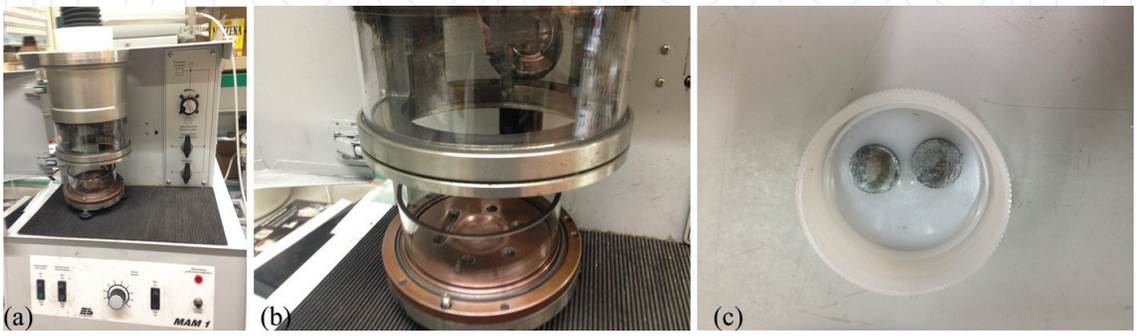

Figure 1. (a) Images of the mini arc furnace and (b) its water-cooled copper crucible, for synthesis of SnSe alloys materials. Pellets of powders of starting material are molten and then quenched in this crucible. (c) Typical disks of as-grown and then pressed intermetallic alloys.

2.3. Microstructural characterization

Surface texture of as-grown pellets was studied by scanning electron microscopy (SEM) in a table-top Hitachi TM-1000 microscope. This microscope, best used for middle and low resolutions with high acceleration voltage, is chiefly used to scan with low magnification to select interesting zones and to study obtain topographical information, with large depth of field, thanks to its sensitivity to surface characteristics.

2.4. Seebeck measurements in home-made apparatus

Measurement of the Seebeck coefficient seems simple: create a temperature gradient and measure the induced voltage. Yet, at elevated temperatures, this poses a challenge, mainly due to large and hard to control temperature gradients.

In many of the instruments used for Seebeck measurement, the most important systematic errors originate in the great difficulty to detect temperatures at exactly the same spot where the voltage difference is observed. Furthermore, the strong chemical and metallurgic reactivity of typical thermoelectric materials at elevated temperatures limits the choice of materials for constructing the instrument. For example, Pt is typically used at high temperatures as an inert and useful material without second thought, but it is out of the question for many thermoelectric alloys of heavy p-block elements. Instead, niobium or tungsten is recommended [42].

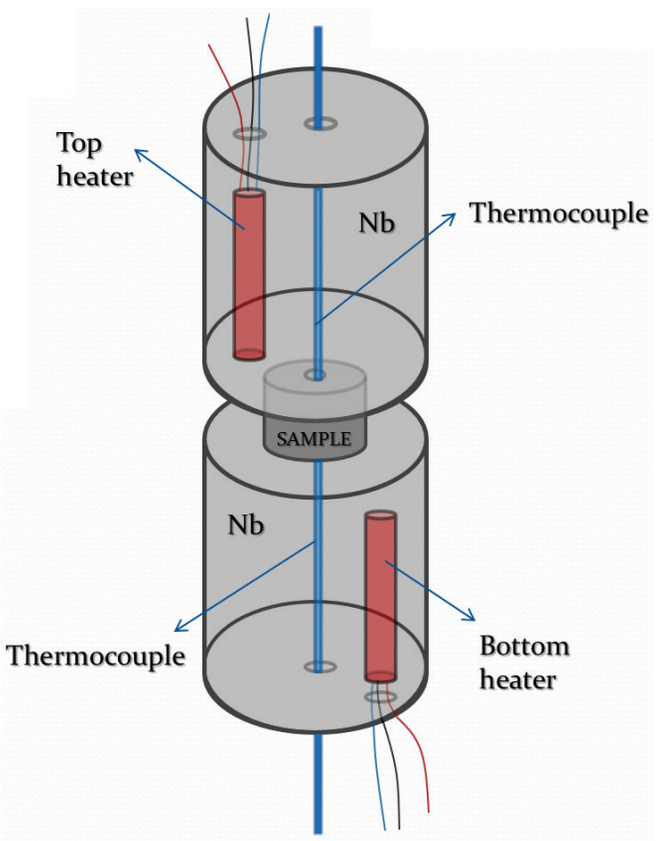

Figure 2. Scheme of the Seebeck measurement apparatus: Two blocks of niobium (Nb) with inner cartridge heaters (with built-in thermocouples), and home-made thermocouples (in contact with the sample).

We try to minimize all the possible errors that could arise during the measurement; for that, we designed a slightly modified device recently published [42]. Using this apparatus, we can measure the Seebeck coefficient from room temperature up to around 950 K. **Figures 2** and **3** show the design scheme of the measurement device. This instrument is composed of two home-made thermocouples, pressed into contact with the sample with springs outside the furnace, two blocks of niobium (Nb), also pressed to the sample by springs, with inner cartridge heaters (with built-in thermocouples), and a tubular furnace with yet another thermocouple.

When high temperature measurements are planned, the system is placed in a vacuum chamber equipped with a turbo-pump, which can reach a vacuum of around 1×10^{-6} mbar. The baseplate is water-cooled in order to provide better control at high temperatures.

Home-made thermocouples are used to measure the temperature of the sample at either side and also the Seebeck voltage. Their election is guided by the need to use inert chemical materials at high temperature against typical compounds in many thermoelectric materials, such as Sn, Pb, Te, and Se. This is the reason we chose thermocouples made of a niobium and chromel combination, ensuring that the Nb wires are in contact with the sample [27, 33], which allows us to reach temperatures near up to 950 K without reactions between samples and thermocouples.

The blocks are built of niobium because i) of its chemical inertness to chalcogenides and pnictides and ii) this metal has a good thermal conductivity, which is important since the heaters are inside them. As an added advantage, the Nb blocks can act as current injection contacts in a 4-point measurement of sample resistance, with the Nb wires of the thermocouples acting as voltage leads, providing an estimate of the electrical conductivity of the material. Although this is not the best geometry to ensure reliable absolute values (the samples have large cross section and are short, just the opposite of what one would desire for 4-point resistivity), it is

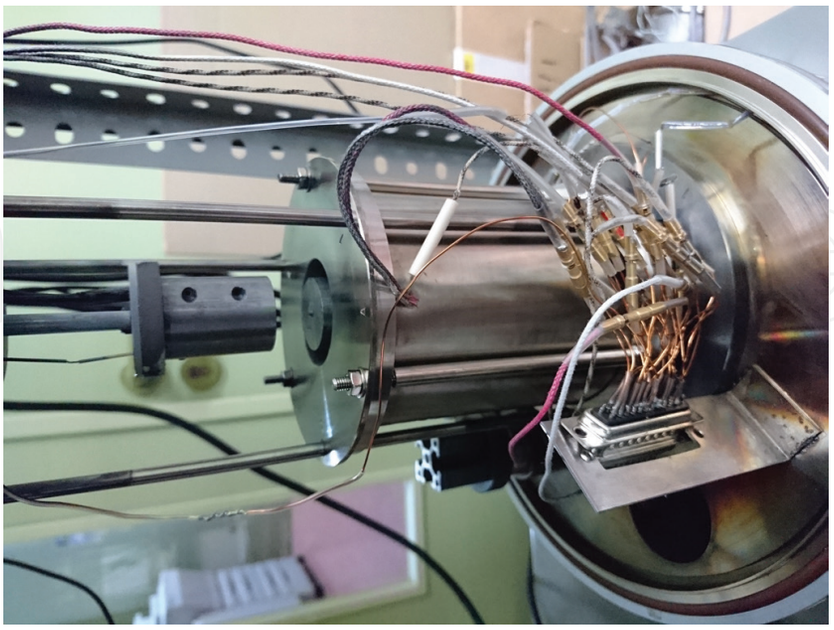

Figure 3. View of the measurement setup, showing the upper and lower Nb pistons and the radiation furnace, which would be shifted upwards during the measurements.

useful to gauge the behavior of the conductivity at higher temperatures. For more reliable absolute conductivity values, we estimated the geometric factor of this setup using a pellet of typical dimensions of our samples (10 mm diameter and 2 mm height) of a commercial Bi_2Te_3 ingot manufactured by TECTEG MFR, by comparing to a conventional in-line 4-point measurement of a 10 × 2 × 2 mm^3 bar cut from the same pellet.

We use a Keithley-2700 scanning multimeter to measure the Seebeck voltage, the thermocouples monitoring the sample temperature, and a Pt sensor used for a numerical "cold" junction compensation. Three independent West-P6100 PID controllers are used to measure and control the cartridge heaters and the furnace. They provide an analog DC programming output of 0–5 V amplified by DeltaES150 DC power supplies. The advantage of this somewhat costlier power control is that the Seebeck voltages and resistivity are less affected by the electronic noise from the heaters. Measurement errors associated with the Seebeck coefficients are close to ~5%, while resistivity error is strongly dependent on the magnitude of the resistance, varying from 20% for low resistances in the mΩ range to negligible errors for values around 1 Ω.

Since typical thermoelectric pellets have resistances in the mΩ range, they are measured using a combination of Keithley Current Source 6221A and a KeithleyNanovoltmeter 2182A. Data acquisition and temperature control are handled by LabVIEW program, which communicates via GPIB with multimeter/nanovoltmeter and via RS485 serial protocol with PID controllers. The whole setup is shown in **Figure 4**.

Figure 4. High temperature Seebeck measurement system: The electronics in the top shelf, the vacuum chamber (with the sample inside) in the back, and the computer with the control-software.

3. Results and discussion

3.1. XRD characterization

Materials of the series $Sn_{1-x}M_xSe$ (M = Ti, Cr, Mn, Zn, Mo, Ag, Cd, Au) were prepared by a simple and straightforward arc-melting technique, yielding highly textured SnSe-type samples. About 2 g ingots were obtained in each case; a part was ground to powder for structural characterization, the remaining pellet was used for transport measurements. XRD patterns are all characteristic of the orthorhombic GeSe structural type, and can be Rietveld-refined in the orthorhombic *Pnma* space group. Both Sn(M) and Se atoms occupy 4*c* (x, ¼, z) positions. Dopant M atoms are distributed at random at Sn positions: different occupation tests were performed in the refinement, verifying M inclusion in the Sn sublattice. **Table 1** includes the unit-cell parameter and volume for each sample; the left panel of **Figure 5a** illustrates the quality of the fit for $Sn_{0.9}Mo_{0.1}Se$, with good discrepancy factors (R_p = 2.29%, R_{wp} = 3.07%, R_{exp} = 1.73%, χ^2 = 3.26, R_{Bragg} = 4.42%). The structure consists of trigonal pyramids $Sn(M)Se_3$ forming double layers perpendicular to the [100] direction, as shown in **Figure 5b**.

Figure 6 illustrates, as an example, the unit cell-volume variation for some selected M dopant atoms. A contraction of the cell is observed when Ag is introduced at Sn positions (**Figure 6a**), whereas the cell volume expands as Ti is introduced in the crystal structure (**Figure 6b**), as a consequence of the different ionic radii of the concerned atoms. In either case, the unit-cell variation assesses the incorporation of the dopant atoms in the crystal structure, discarding the inclusion of spurious phases in the grain boundaries or as secondary phases.

3.2. Scanning electron microscopy (SEM)

The layered crystal structure of SnSe-type compounds, containing strong covalent bonds within the layers, and much weaker interactions between adjacent layers, promotes the easy cleavage of materials. The arc-furnace procedure, involving a fast quenching of the samples from the molten state, drives a peculiar microstructure consisting of piles of stacking sheets, as shown in **Figure 7**.

Illustrated for M = Mn and M = Cd, the same typical microstructure is observed for all the samples. We find individual sheets with thickness below 0.1 μm (typically 20 to 40 nm). This micro- or nanostructuration has strong influence on the thermoelectric properties, especially the many surface boundaries that are responsible for scattering of both charge carriers and phonons (i.e. the electrical and the thermal conductivity).

3.3. Transport measurements

The Seebeck coefficient and electrical conductivity were measured in coin-shaped pellets of 12 mm diameter in the home-made device described before. **Table 1** includes the thermopower and electrical conductivity at room temperature (RT) for all the studied samples, which is useful

Material	Seebeck coefficient (μV/K)	Electrical conductivity (S/m)	Lattice constant a (Å)	Lattice constant b (Å)	Lattice constant c (Å)	Volume (Å^3)
SnSe	403	13	11.500 (2)	4.151 (1)	4.443 (1)	212.04 (9)
SnSe (SPS)	316	0.7	11.502 (2)	4.1539 (8)	4.4441 (9)	212.33 (7)
$Sn_{0.9}Y_{0.1}Se$	−81	6	11.503 (3)	4.157 (1)	4.436 (2)	212.1 (1)
$Sn_{0.95}Ti_{0.05}Se$	12	111	11.497 (2)	4.1531 (8)	4.443 (1)	212.14 (7)
$Sn_{0.90}Ti_{0.10}Se$			11.523 (7)	4.165 (3)	4.430 (3)	212.6 (3)
$Sn_{0.85}Ti_{0.15}Se$	7	2841	11.508 (4)	4.155 (1)	4.448 (2)	212.7 (1)
$Sn_{0.95}Cr_{0.05}Se$	−2	174	11.494 (3)	4.151 (1)	4.440 (1)	211.8 (1)
$Sn_{0.9}Cr_{0.1}Se$	−5	251	11.495 (3)	4.151 (1)	4.441 (1)	211.9 (1)
$Sn_{0.99}Mo_{0.01}Se$	480	4	11.492 (2)	4.1516 (7)	4.4424 (9)	211.94 (6)
$Sn_{0.97}Mo_{0.03}Se$	500	8	11.502 (2)	4.1560 (8)	4.446 (1)	212.53 (7)
$Sn_{0.95}Mo_{0.05}Se$	280	15	11.499 (2)	4.1529 (8)	4.445 (1)	212.29 (7)
$Sn_{0.9}Mo_{0.1}Se$	442	3	11.502 (2)	4.1523(8)	4.445 (1)	212.29 (7)
$Sn_{0.8}Mo_{0.2}Se$	404	8	11.504 (2)	4.1553 (9)	4.445 (1)	212.51 (8)
$Sn_{0.7}Mo_{0.3}Se$	357	47	11.504 (2)	4.155 (1)	4.444 (1)	212.41 (8)
$Sn_{0.99}Mn_{0.01}Se$	453	42	11.509 (2)	4.1558 (8)	4.447 (1)	212.72 (8)
$Sn_{0.99}Ag_{0.01}Se$	220	330	11.505 (2)	4.155 (1)	4.446 (1)	212.57 (9)
$Sn_{0.97}Ag_{0.03}Se$	161	111	11.500 (2)	4.1553 (9)	4.445 (1)	212.42 (8)
$Sn_{0.95}Ag_{0.05}Se$	112	276	11.502 (2)	4.155(1)	4.445 (1)	212.40 (9)
$Sn_{0.9}Ag_{0.1}Se$	123	3411	11.496 (4)	4.152 (2)	4.441 (2)	212.0 (2)
$Sn_{0.99}Au_{0.01}Se$	368	224	11.506 (3)	4.155 (1)	4.446 (1)	212.6 (1)
$Sn_{0.9}Zn_{0.1}Se$	432	18	11.500 (4)	4.154 (1)	4.444 (2)	212.3 (1)
$Sn_{0.99}Cd_{0.01}Se$	590	2	11.502 (3)	4.153 (1)	4.443 (2)	212.2 (1)
$Sn_{0.97}Cd_{0.03}Se$	640	0.7	11.497 (3)	4.152 (1)	4.440 (2)	211.9 (1)
$Sn_{0.95}Cd_{0.05}Se$	549	4	11.503 (3)	4.154 (1)	4.441 (1)	212.2 (1)
$Sn_{0.9}Cd_{0.1}Se$	482	23	11.513 (3)	4.161 (1)	4.444 (2)	212.9 (1)
$Sn_{0.8}Cd_{0.2}Se$	508	6	11.506 (3)	4.156 (1)	4.441 (2)	212.4 (1)

Table 1. Seebeck coefficient, electrical conductivity, and unit cell parameters of the different $Sn_{1-x}M_xSe$ alloys measured at room temperature.

as a preliminary screening in order to avoid particularly time-consuming high-temperature measurements. For the sake of comparison, some samples were also prepared by ball milling followed by SPS processes; inferior (lower) Seebeck coefficients and (considerably lower) electrical conductivities were invariably obtained, proving the excellence of the arc-melting procedure

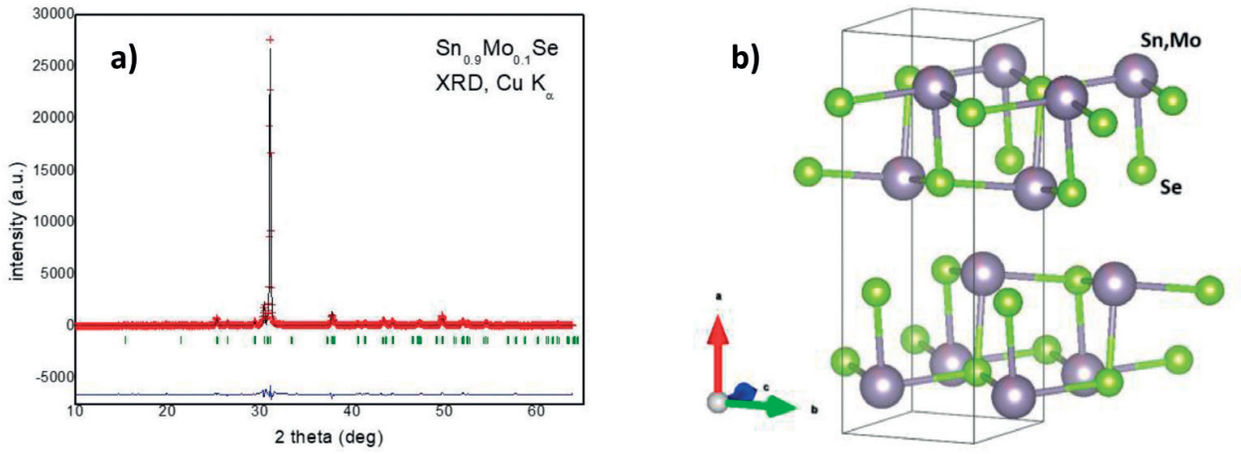

Figure 5. (a) XRD pattern and its Rietveld-refinement of $Sn_{0.9}Mo_{0.1}Se$, showing an excellent agreement between observed (crosses) and calculated (black line) profiles. (b) View of the $Sn_{1-x}Mo_xSe$ crystal structure, highlighting the layers of $Sn(Mo)Se_3$ polyhedra perpendicular to **a** axis.

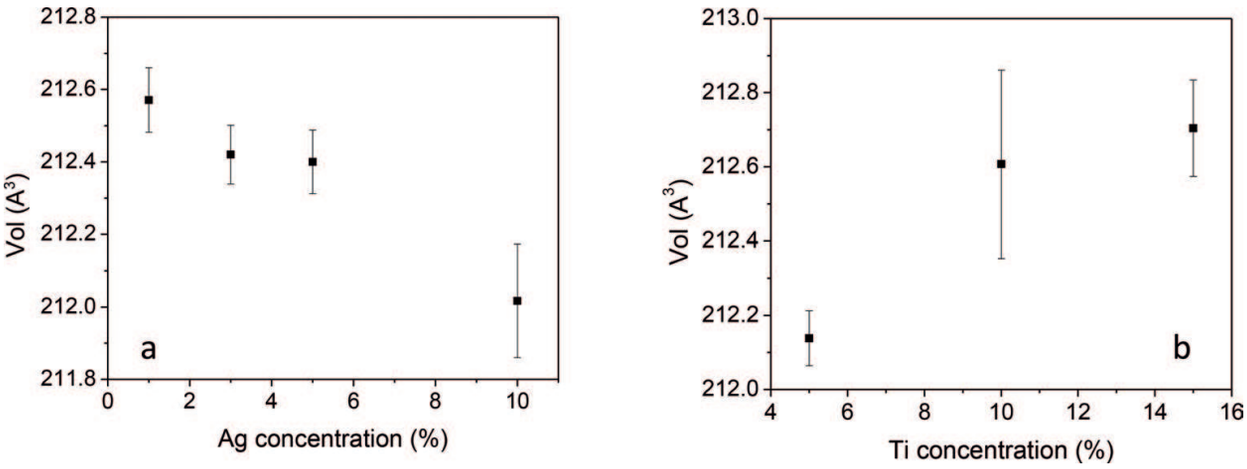

Figure 6. Unit-cell volume variation with the concentration of dopant element for (a) Ag and (b) Ti.

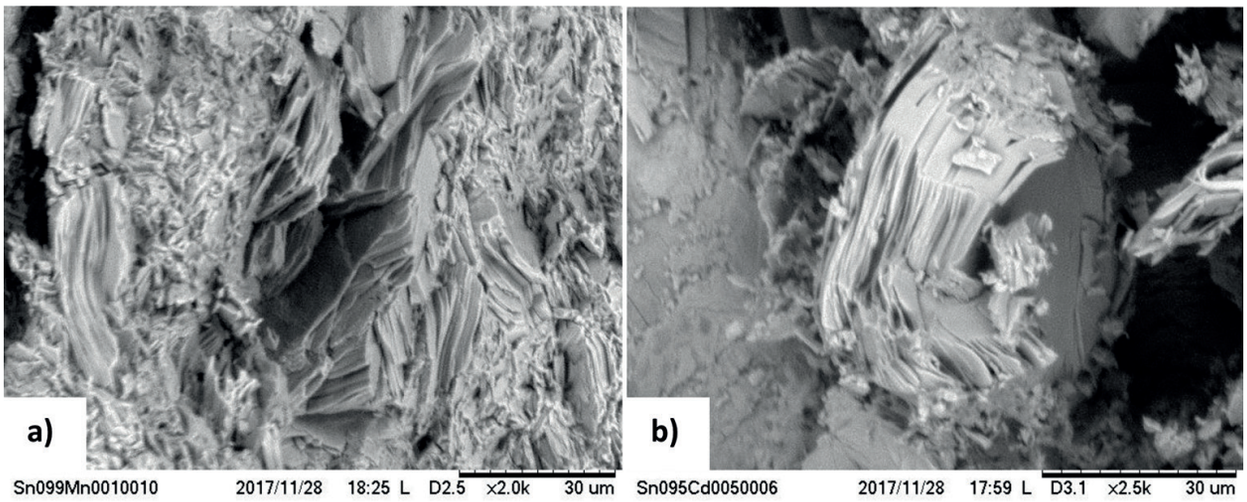

Figure 7. SEM image of as-grown $Sn_{1-x}M_xSe$, exhibiting nanostructuration, consisting of piles of nanometric platelets (perpendicular to [100] direction) taken with (a) 2000 magnification for M = Mn and (b) 2500 magnification for M = Cd.

reported here. Some samples were subsequently chosen for a more detailed high temperature study, up to 950 K.

As mentioned in the Introduction, pure tin selenide has good thermoelectric properties at high temperature [18]. However, in our screening we focus on the room temperature properties, and although we observed a high Seebeck coefficient, its electrical conductivity turned out to be much lower, by one or two orders of magnitude, than in single crystals. A good reference value for the electrical conductivity would be above 1000 S/m. Our approach has been to enhance this state of affairs by doping SnSe with adequate elements to boost the RT electrical conductivity, while keeping a good Seebeck coefficient. The thermoelectric performance is certainly enhanced at elevated temperature, as we indeed observe here. In addition, doping elements that yield almost zero Seebeck coefficient but good electrical conductivity are very promising for further optimization at much lower doping concentrations, such as the case of Ti, or Cr.

From **Table 1**, it is noteworthy that certain doping elements such as Mo or Cd are able to enhance the RT Seebeck coefficient to as high as 480 μV/K ($Mo_{0.01}$), 500 μV/K ($Mo_{0.03}$), 590 μV/K ($Cd_{0.01}$) or even 640 μV/K ($Cd_{0.03}$), while other elements such as Cr kill the thermoelectric performance (−2 μV/K for $Cr_{0.05}$). The microscopic origin of this behavior is beyond this study, since our aim was the preliminary identification of those doping elements that induce a better performance. Some selected samples with promising properties were studied above room temperature and are described in the following sections.

3.3.1. $Sn_{0.9}Y_{0.1}Se$

Starting from the left of the periodic table, we have alloyed SnSe with 10% yttrium, to obtain $Sn_{0.9}Y_{0.1}Se$. Interestingly, it turns out to be an n-type semiconductor, with negative Seebeck coefficient, at room temperature. The thermal evolution of the Seebeck coefficient and the electrical conductivity are shown in **Figure 8a**.

The Seebeck coefficient changes sign around 600 K. This sign change is reversible, reproducible in the same sample, and was observed in several specimens. The explanation has to do with a scenario where negative and positive carriers coexist in the material. At lower temperatures electrons are the majority carriers and holes the minority carriers. At higher temperatures, more holes are excited, in such a way that holes become the majority carriers, dominating their contribution to the Seebeck effect, turning it positive. This might happen, for example, if a narrow band of defects lies near the top of the valence band with the Fermi-level trapped near its bottom.

The electrical conductivity of $Sn_{0.9}Y_{0.1}Se$ rises exponentially with temperature, corresponding to a thermally activated semiconductor with an activation energy of E_g~0.2 eV, obtained from the inset of **Figure 8c**. The excellent fit shows that, despite the geometry utilized in the home-made apparatus, it provides highly reliable temperature-dependent relative conductivity values. Such a small band-gap is not intrinsic to pure SnSe. It may correspond to the above-mentioned defect band. Another possibility is that the electrical conductivity, invariably poor in arc-melting produced SnSe, and its alloys, at room temperature [36–39], is limited by intergrain hopping with activation energy of around 0.2 eV.

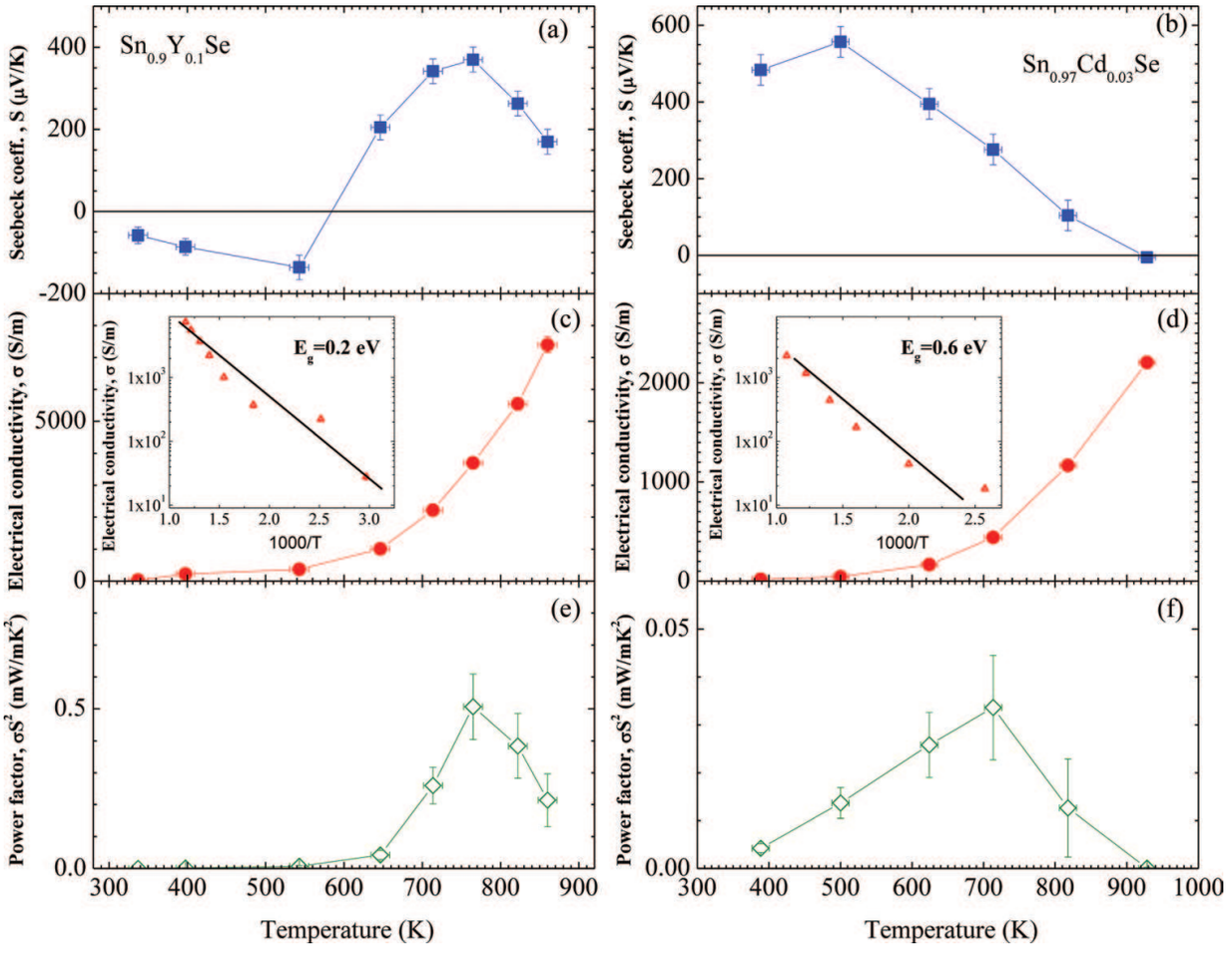

Figure 8. (a) Seebeck coefficient, (c) electrical conductivity, (e) power factor of $Sn_{0.9}Y_{0.1}Se$, and (b) Seebeck coefficient, (d) electrical conductivity, (f) power factor of $Sn_{0.97}Cd_{0.03}Se$ and insert in (d) inverse semilog-plot of electrical conductivity indicating a gap.

The power factor reaches a maximum of 0.5 mW/mK^2 at around 800 K. As we will show below and have published before [36–39], the thermal conductivity for SnSe alloys produced by arc-melting is less than 0.5 W/mK, indicating a possible figure of merit zT > 0.8 for $Sn_{0.9}Y_{0.1}Se$.

3.3.2. $Sn_{0.97}Cd_{0.03}Se$

As an alloy with contrasting behavior, we show the transport properties of $Sn_{0.97}Cd_{0.03}Se$ (**Figure 8b**, **d**, **f**). The cadmium-doped SnSe is the system with the highest Seebeck coefficients in this study (**Table 1**). Conversely, the electrical conductivity is very poor at RT, but there is an extraordinary increase with temperature, as illustrated in **Figure 8** on the right (middle panel). Both the large Seebeck coefficient and the low electrical conductivity indicate very low charge concentration. The steady decrease of the Seebeck coefficient (highest at 500 K with 570 μV/K) accompanied by the rapid increase of the electrical conductivity is another manifestation of the Pisarenko relationship [6]. The exponential temperature dependence of σ indicates a gap of E_g = 0.6 eV. This is very similar to the intrinsic gap of SnSe. We can conclude from this study that Cd is unlikely to be a useful dopant for SnSe

since its power factor is rather small, probably because of a lack of effective charge transfer (i.e. doping).

3.3.3. $Sn_{0.95}Mo_{0.05}Se$

We have prepared a series of molybdenum-alloyed SnSe samples at various concentrations, from 1% up to 30% Mo. According to the change of lattice parameters, Mo clearly enters the SnSe structure. However, the dependence of any of the properties studied (Seebeck coefficient, electrical conductivity, unit-cell volume) vary non-monotonously, thus the use of Mo as an alloying element is questionable. Without more detailed structural studies it is impossible to assess whether Mo indeed incorporates at the nominal compositions into SnSe. For 5% Mo-doped SnSe, the temperature-dependent Seebeck coefficient is shown in **Figure 9a**. The Seebeck coefficient is positive and reaches a maximum of 400 μV/K around 700 K. While the samples are rather resistive at room temperature, we observed an abrupt increment of the electrical conductivity at 800 K, reaching values up to perhaps 10,000 S/m (not shown).

3.3.4. $Sn_{0.99}Mn_{0.01}Se$

For SnSe doped with 1% manganese (**Figure 9b**), we also find an abrupt change of sign of the Seebeck coefficient, as described above for $Sn_{0.9}Y_{0.1}Se$. However, for Mn-doped SnSe the thermoelectric power is positive at low temperatures, and inverts above 630 K. A similar explanation considering two types of charge carriers may be invoked here. Importantly, this behavior is intrinsic to the material, not an effect of thermally induced chemical changes, as it is reversible, and reproducible in several thermal cycles. Therefore, Mn-doping provides a high temperature n-type SnSe thermoelectric element.

3.3.5. $Sn_{0.9}Ag_{0.1}Se$

The Ag-doped SnSe system is an example where the interplay of the Seebeck coefficient and electrical conductivity follows the Pisarenko relation, in **Table 1**. For low Ag-doping the Seebeck coefficient is around 200 μV/K at room temperature with an electrical conductivity

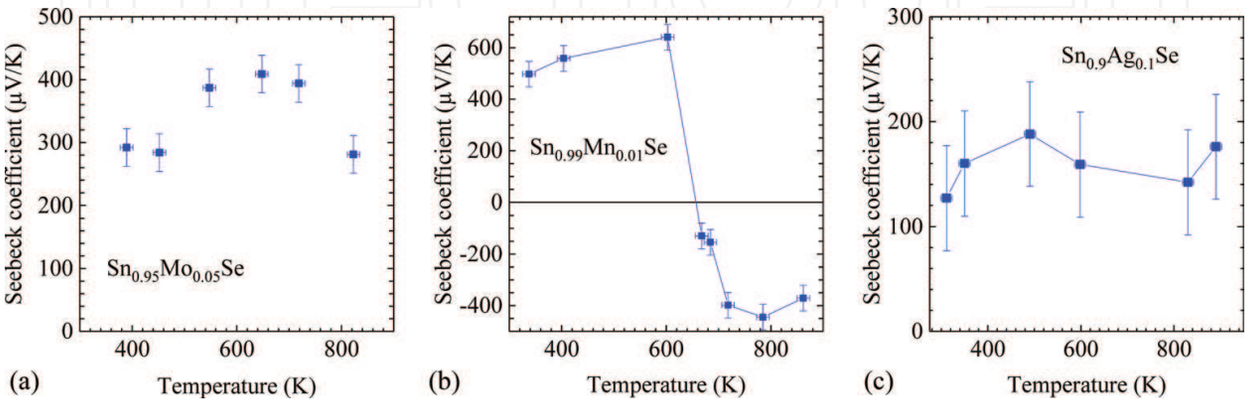

Figure 9. Seebeck coefficient of (a) $Sn_{0.95}Mo_{0.05}Se$, (b) $Sn_{0.99}Mn_{0.01}Se$, and (c) $Sn_{0.9}Ag_{0.1}Se$.

around 100 S/m, but for 10% Ag (itself difficult to stabilize by other methods [21]), while the Seebeck coefficient halves, σ shoots up to above 3000 S/m. That the Ag indeed enters the structure at such high doping levels is shown up by the continuous decrease of the unit-cell volume in **Figure 6a**. A σ increase of several orders of magnitude with respect to the RT value was observed above 800 K. The Seebeck coefficient remained stable between 150 and 200 μV/K (within the error bars), indicating that the conductivity is limited by intergrain boundaries. This effect is seen also in the small gap of a gold-doped alloy (**Figure 10**), as well as in the Y-doped sample in **Figure 8c**.

3.3.6. $Sn_{0.99}Au_{0.01}Se$

Gold doping is a yet-unexplored alternative to silver doping. The transport results corresponding to SnSe doped with 1% Au are shown in **Figure 10**. The Seebeck coefficient increases

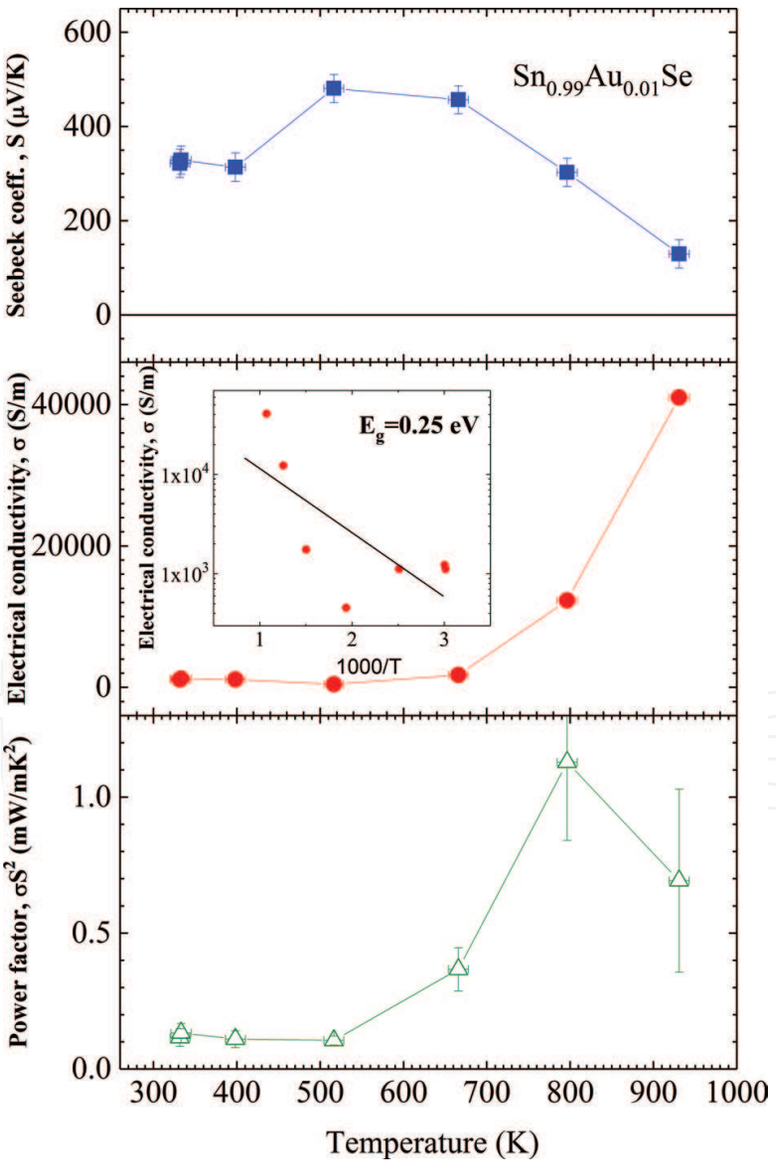

Figure 10. $Sn_{0.99}Au_{0.01}Se$: (top) Seebeck coefficient, (middle) electrical conductivity, (bottom) power factor, and (insert) inverse semilog plot of electrical conductivity indicating a gap.

up to a maximum at 500 K reaching 500 μV/K. The ambient electrical conductivity is noticeably lower than for Ag, yet it steadily increases with temperature reaching 40,000 S/m at 950 K, with a maximum power factor around 800 K above 1 mW/mK^2, thus implying a maximum zT up to 1.5 (this surprising value requires more careful verification of the resistivity measurements). The exponential increase of sigma indicates a gap of Eg = 0.25 eV, similar to the one seen in the Y-doped sample in **Figure 8**. Such a small gap, together with the relatively constant Seebeck coefficient, indicates that it is not the charge concentration increase, but thermally activated intergrain hopping limits the electrical conductivity in arc-molten SnSe.

3.4. Thermal conductivity

Figure 11 illustrates the total thermal conductivity (κ) obtained by laser-flash diffusivity method for two selected thermoelectric compounds: $Sn_{0.99}Mn_{0.01}Se$ and $Sn_{0.95}Ti_{0.05}Se$; in our experience, SnSe alloys prepared by arc-melting have similar thermal conductivities, and these values are representative for other alloys and different compositions.

Both SnSe alloys display remarkably low thermal conductivities at high-temperature region. At room temperature the thermal conductivities are 0.95 and 0.88 W/mK for the Mn and Ti alloys, respectively. These decrease further with increasing temperature, reaching 0.4 W/mK at 675 K. Both electron and phonon transport contribute to the total thermal conductivity, denoted as lattice thermal conductivity (κ_{lat}) due to phonon transport, and charge thermal conductivity (κ_{ch}) due to thermal transport of charges (electrons and/or holes). With the use

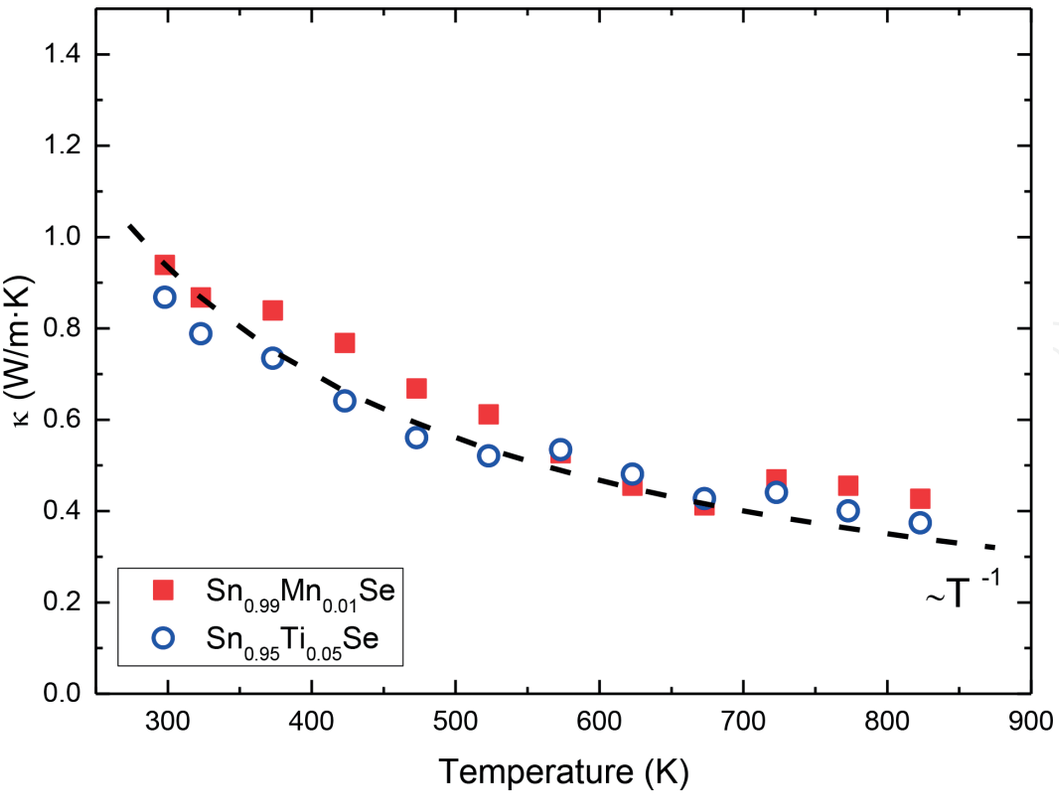

Figure 11. Thermal conductivity of $Sn_{0.99}Mn_{0.01}Se$ and $Sn_{0.95}Ti_{0.05}Se$ obtained by laser flash diffusivity. The black-dashed line indicates the classical behavior, $\kappa \sim T^{-1}$, due to the phonon-phonon interaction.

of the Wiedemann-Franz law [7], we can estimate charge contribution to the thermal conductivity as a function of temperature, $\kappa_{ch} = L_0 T\sigma$, with L_0 the Lorentz number and σ the electrical conductivity. For the highly resistive SnSe and its alloys, total thermal conductivity is dominated by the lattice thermal conductivity by a factor of 10,000:1. The temperature dependence of the lattice thermal conductivity follows the T^{-1} trend (black-dashed line in **Figure 11**), showing that the phonon-phonon interaction dominates in this temperature range.

The extremely low thermal conductivities observed in all the materials of the different doped series reported here afford considerably high figures of merit, zT.

4. Conclusion

We propose arc-melting technique as a fast one-step process to elaborate nanostructured intermetallic alloys of the $Sn_{1-x}M_xSe$ family (M: transition metals). All the specimens show a peculiar microstructure consisting of stacks of nanosheets. The presence of many extended grain boundaries perturbs the propagation of phonons and brings about extremely low thermal conductivities, around 0.5 W/mK. Using as quick screening tool the RT Seebeck coefficient and electrical conductivity, our preliminary survey of different SnSe-related transition metal alloys shows very distinct behaviors: certain doping elements such as Mo or Cd are able to enhance the RT Seebeck coefficient to values as high as 640 μV/K (3% Cd), while other elements such as Cr practically kill the thermoelectric performance (−2 μV/K for 5% Cr). The microscopic origin of this diverse behavior is far from being understood. Crucially, we find that some dopants, such as Y and Mn, can provide n-type alloys with a change of sign of the Seebeck coefficient. $Sn_{0.90}Y_{0.10}Se$ is n-type at low temperature and changes to p-type around 600 K. This sign change is reversible, and this behavior was reproduced in several specimens. The opposite behavior is observed for $Sn_{0.99}Mn_{0.01}Se$, which changes from p-type to n-type above 630 K. Many materials showed evidence of the Pisarenko relationship at work: dopants that, at some concentration, can yield highly conducting samples, usually with almost zero Seebeck coefficient, whereas for pure or lightly doped SnSe alloys bad conduction with large Seebeck effects are observed. This rich phenomenology can be useful as a guide for further, deeper research. We also describe an instrument to characterize the high-temperature Seebeck coefficient and electrical conductivity in disk-shaped pellets directly obtained from the intermetallic ingots. Problems with alloying of the samples at high temperature are avoided by the use of Nb pistons and Nb-based thermocouples that are chemically inert to reactive p-block elements. This is shown to be essential for the accuracy and reproducibility of the measurements, avoiding the degradation of the materials after thermally cycling up to 950 K.

In the context of thermoelectric devices, our finding of stable n-type doped SnSe at elevated temperatures prepared by a straightforward method would allow the use of SnSe derivatives for high-temperature applications. Thermoelectric devices require both n- and p-type semiconductors with matching thermoelectric, electronic, and mechanical properties, and this material system based on SnSe alloys could find application, for example, in the exhaust heat recovery or in solar-hybrid TEG applications.

Acknowledgements

We thank the financial support of the Spanish Ministry of Science and Innovation to the project MAT2017–84496-R.

Author details

Javier Gainza[1], Federico Serrano-Sánchez[1], Mouna Gharsallah[1,2], Manuel Funes[1], Félix Carrascoso[1], Norbert M. Nemes[3], Oscar J. Dura[4], José L. Martínez[1] and José A. Alonso[1]*

*Address all correspondence to: ja.alonso@icmm.csic.es

1 Instituto de Ciencia de Materiales de Madrid, C.S.I.C., Madrid, Spain

2 National School of Engineers, Sfax University, Tunisia

3 Departamento de Física de Materiales, Universidad Complutense de Madrid, Madrid, Spain

4 Departamento Física Aplicada and INEI, Universidad de Castilla La Mancha, Ciudad Real, Spain

References

[1] Rowe DM. CRC Handbook of Thermoelectrics. CRD Press; 1995. DOI: 10.1201/9781420049718.ch3

[2] Goldsmid HJ. Introduction to thermoelectricity. SSMATERIALS, volume 121. Springer-Verlag Berlin Heidelberg; 2016. DOI: 10.1007/978-3-662-49256-7

[3] Chen G, Dresselhaus MS, Dresselhaus G, et al. Recent developments in thermoelectric materials. International Materials Review. 2003;**48**:45-66. DOI: 10.1179/095066003225010182

[4] Nolas GS, Sharp J, Goldsmid HJ. Thermoelectrics: Basic Principles and New Materials Developments. New York: Springer; 2001

[5] Rull-Bravo M, Moure A, Fernández JF, Martín-González M. Skutterudites as thermoelectric materials: Revisited. RSC Advances. 2015;**5**:41653-41667. DOI: 10.1039/C5RA03942H

[6] Ioffe AF. Physics of Semiconductors. New York: Academic Press; 1960

[7] Zaitsev VK, Fedorov MI, Eremin IS, Gurieva EA, Rowe DW. Thermoelectrics Handbook: Macro to Nano. Boca Ratonp: CRC press; 2006

[8] Kim HS, Gibbs ZM, Tang Y, et al. Characterization of Lorenz number with Seebeck coefficient measurement. APL Mater. 2015;**3**:41506. DOI: 10.1063/1.4908244

[9] DiSalvo F. Thermoelectric cooling and power generation. Science. 1999;**285**:703-706. DOI: 10.1126/science.285.5428.703

[10] Zebarjadi M, Esfarjani K, Dresselhaus MS, et al. Perspectives on thermoelectrics: From fundamentals to device applications. Energy & Environmental Science. 2012;**5**:5147-5162. DOI: 10.1039/C1EE02497C

[11] Ong KS. Review of solar, heat pipe and thermoelectric hybrid systems for power generation and heating. International Journal of Low-Carbon Technologies. 2015;**11**:460-465. DOI: 10.1093/ijlct/ctv022

[12] Orr B, Akbarzadeh A, Mochizuki M, Singh R. A review of car waste heat recovery systems utilising thermoelectric generators and heat pipes. Applied Thermal Engineering. 2016;**101**:490-495. DOI: 10.1016/j.applthermaleng.2015.10.081

[13] Quan R, Liu G, Wang C, et al. Performance investigation of an exhaust thermoelectric generator for military SUV application. Coatings. 2018;**8**:45. DOI: 10.3390/coatings8010045

[14] Kumar S, Heister SD, Xu X, et al. Thermoelectric generators for automotive waste heat recovery systems part I: Numerical modeling and baseline model analysis. Journal of Electronic Materials. 2013;**42**:665-674. DOI: 10.1007/s11664-013-2471-9

[15] Nolas GS, Poon J, Kanatzidis M. Recent developments in bulk thermoelectric materials. MRS Bulletin. 2006;**31**:199-205. DOI: 10.1557/mrs2006.45

[16] Zhang X, Zhao L-D. Thermoelectric materials: Energy conversion between heat and electricity. Journal of Materials. 2015;**1**:92-105. DOI: 10.1016/j.jmat.2015.01.001

[17] Snyder GJ, Toberer ES. Complex thermoelectric materials. Nature Materials. 2008;**7**:105-114. DOI: 10.1038/nmat2090

[18] Zhao L-D, Lo S-H, Zhang Y, et al. Ultralow thermal conductivity and high thermoelectric figure of merit in SnSe crystals. Nature. 2014;**508**:373-377. DOI: 10.1038/nature13184

[19] Sassi S, Candolfi C, Vaney JB, et al. Assessment of the thermoelectric performance of polycrystalline p -type SnSe. Applied Physics Letters. 2014;**104**:212105. DOI: 10.1063/1.4880817

[20] Chen S, Cai K, Zhao W. The effect of Te doping on the electronic structure and thermoelectric properties of SnSe. Physica B: Condensed Matter. 2012;**407**:4154-4159. DOI: 10.1016/j.physb.2012.06.041

[21] Chen C-L, Wang H, Chen Y-Y, et al. Thermoelectric properties of p-type polycrystalline SnSe doped with Ag. Journal of Materials Chemistry A. 2014;**2**:11171-11176. DOI: 10.1039/c4ta01643b

[22] Castellanos-Gomez A. Black phosphorus: Narrow gap, wide applications. Journal of Physical Chemistry Letters. 2015;**6**:4280-4291. DOI: 10.1021/acs.jpclett.5b01686

[23] Heremans JP, Wiendlocha B, Chamoire AM. Resonant levels in bulk thermoelectric semiconductors. Energy & Environmental Science. 2012;**5**:5510-5530. DOI: 10.1039/C1EE02612G

[24] Zhang Q, Chere EK, Sun J, et al. Studies on thermoelectric properties of n-type polycrystalline SnSe1-xSx by iodine doping. Advanced Energy Materials. 2015;**5**:1500360. DOI: 10.1002/aenm.201500360

[25] Kutorasinski K, Wiendlocha B, Kaprzyk S, Tobola J. Electronic structure and thermoelectric properties of n- and p-type SnSe from first-principles calculations. Physical Review B. 2015;**91**:1-12. DOI: 10.1103/PhysRevB.91.205201

[26] Li CW, Hong J, May AF, et al. Orbitally driven giant phonon anharmonicity in SnSe. Nature Physics. 2015;**11**:1-8. DOI: 10.1038/nphys3492

[27] Guo R, Wang X, Kuang Y, Huang B. First-principles study of anisotropic thermoelectric transport properties of IV–VI semiconductor compounds SnSe and SnS. Physical Review B: Condensed Matter and Materials Physics. 2015;**92**:1-13. DOI: 10.1103/PhysRevB.92.115202

[28] Fu Y, Xu J, Liu G-Q, et al. Enhanced thermoelectric performance in p-type polycrystalline SnSe benefiting from texture modulation. Journal of Materials Chemistry C. 2016;**4**:1201-1207. DOI: 10.1039/C5TC03652F

[29] Zhao L-D, Chang C, Tan G, Kanatzidis M. SnSe: A remarkable new thermoelectric material. Energy & Environmental Science. 2016;**9**(10):15-17. DOI: 10.1039/C6EE01755J

[30] Peng K, Lu X, Zhan H, et al. Broad temperature plateau for high ZTs in heavily doped p-type SnSe single crystals. Energy & Environmental Science. 2016;**9**:454-460. DOI: 10.1039/C5EE03366G

[31] Chen YX, Ge ZH, Yin M, et al. Understanding of the extremely low thermal conductivity in high-performance polycrystalline SnSe through potassium doping. Advanced Functional Materials. 2016;**26**:6836-6845. DOI: 10.1002/adfm.201602652

[32] Dai XQ, Wang XL, Li W, Wang TX. Electronic properties of the SnSe-metal contacts: First-principles study. Chinese Physics B. 2015;**24**:7-12. DOI: 10.1088/1674-1056/24/11/117308

[33] Kim Y, Yoon G, Cho BJ, Park SH. Multi-layer metallization structure development for highly efficient polycrystalline SnSe thermoelectric devices. Applied Sciences. 2017;**7**:1116. DOI: 10.3390/app7111116

[34] Zhao L, Tan G, Hao S, et al. Ultrahigh power factor and thermoelectric performance in hole-doped single-crystal SnSe. Science. 2016;**351**:141. DOI: 10.1126/science.aad3749

[35] Duong AT, Nguyen VQ, Duvjir G, et al. Achieving ZT = 2.2 with Bi-doped n-type SnSe single crystals. Nature Communications. 2016;**7**:1-6. DOI: 10.1038/ncomms13713

[36] Serrano-Sánchez F, Gharsallah M, Bermúdez J, et al. Nanostructured state-of-the-art thermoelectric materials prepared by straight-forward arc-melting method. Thermoelectrics for Power Generation – A Look at Trends in the Technology. InTech-Open Access Publisher; December 21, 2016. http://www.intechopen.com/books/thermoelectrics-for-power-generation-a-look-at-trends-in-the-technology DOI: 10.5772/65115

[37] Serrano-Sánchez F, Gharsallah M, Nemes NM, et al. Record Seebeck coefficient and extremely low thermal conductivity in nanostructured SnSe. Applied Physics Letters. 2015;**106**:83902. DOI: 10.1063/1.4913260

[38] Serrano-Sanchez F, Nemes NM, Dura OJ, et al. Structural phase transition in polycrystalline SnSe: A neutron diffraction study in correlation with thermoelectric properties. Journal of Applied Crystallography. 2016;**49**:2138-2144. DOI: 10.1107/S1600576716015405

[39] Gharsallah M, Serrano-Sánchez F, Nemes NM, et al. Giant seebeck effect in Ge-doped SnSe. Scientific Reports. 2016;**6**:26774. DOI: 10.1038/srep26774

[40] Lan Y, Minnich AJ, Chen G, Ren Z. Enhancement of thermoelectric figure-of-merit by a bulk Nanostructuring approach. Advanced Functional Materials. 2010;**20**:357-376. DOI: 10.1002/adfm.200901512

[41] Rodríguez-Carvajal J. Recent advances in magnetic structure determination by neutron powder diffraction. Physics B. 1993;**192**:55-69. DOI: 10.1016/0921-4526(93)90108-I

[42] Iwanaga S, Toberer ES, Lalonde A, Snyder GJ. A high temperature apparatus for measurement of the Seebeck coefficient. The Review of Scientific Instruments. 2011;**82**:63905. DOI: 10.1063/1.3601358